Alternative method to deduce bubble dynamics in single-bubble sonoluminescence experiments

G. Simon[1] and M. T. Levinsen[2]
[1]*Department of Atomic Physics, Eötvös Loránd University, H-1117 Budapest, Hungary*
[2]*Center for Chaos and Turbulence Studies, Niels Bohr Institute, Blegdamsvej 17 DK 2100, Copenhagen Ø, Denmark*
(Received 6 September 2002; published 27 February 2003)

In this paper we present an experimental approach that allows to deduce the important dynamical parameters of single sonoluminescing bubbles (pressure amplitude, ambient radius, radius-time curve). The technique is based on a few previously confirmed theoretical assumptions and requires the knowledge of quantities such as the amplitude of the electric excitation and the phase of the flashes in the acoustic period. These quantities are easily measurable by a digital oscilloscope, avoiding the cost of the expensive lasers or ultrafast cameras of previous methods. We show the technique in a particular example and compare the results with conventional Mie scattering. We find that within the experimental uncertainties these two techniques provide similar results.

DOI: 10.1103/PhysRevE.67.026320 PACS number(s): 47.55.Dz, 43.25.+y, 78.60.Mq

I. INTRODUCTION

Single-bubble sonoluminescence (SBSL) is a physical process where an oscillating gas bubble levitated acoustically in a host liquid emits brief flashes of light in each period of the harmonic excitation [1]. In experiments, bubble levitation is done in resonators the size of a jar, filled with liquid, and the acoustic excitation is accomplished by piezoelectric transmitters (PZT) [2]. The study of SBSL is motivated by the fact that through it one can study physical processes and the properties of matter at extreme conditions of high density, pressure, and temperature. The variety of processes associated with the phenomenon include heat [3] and mass [4] transfer, chemical reactions [5], shape oscillations [6], chaos [7], shock-wave emission [8], and light emission [9] to name a few.

In order to validate theories of SBSL it is crucial to be able to measure several important parameters, such as the pressure amplitude near the bubble, P_a, the ambient radius R_0, or the radius-time curve $R(t)$ in an acoustic period. Previous methods to measure these quantities are variations of the Mie scattering technique [10], direct imaging of the bubble [11], differential light scattering [12], and a method based on the Doppler effect [13]. The common factor in these methods is that each of them requires a rather sophisticated and expensive experimental setup including lasers, precision optics, and high-speed cameras. Moreover each of these methods are *invasive*, i.e., they involve external action in the measuring process (e.g., laser or back-lighting), which may disturb the measurement of some other features of SBSL. The quantity P_a can also be measured directly by a needle hydrophone; however, because of the intrusive nature, high cost, and relatively low precision of this, P_a is usually deduced from fitting measured $R(t)$ curves to the solutions of the Rayleigh-Plesset equation, which describes the dynamics of the bubble's volumetric oscillations.

These methods confirmed several theoretically predicted features of SBSL, for example, that stable light-emitting bubbles obey diffusive and chemical stability [14–16]. In a previous study [17] we exploited this fact to develop a technique to deduce P_a, R_0, or $R(t)$. Here we elaborate on our method in more detail, present its advantages and limitations and compare its results with Mie scattering.

II. DESCRIPTION OF THE FITTING TECHNIQUE

Our technique is based on the following assumptions:

(1) The dynamics of the bubble wall $R(t)$ is well described by the Rayleigh-Plesset (RP) equation

$$R\ddot{R}+\frac{3}{2}\dot{R}^2=\frac{1}{\rho}[P_g(R(t))-P_f(t)-P_0+P_v] + \frac{R}{\rho c}\frac{d}{dt}[P_g(R(t))-P_f(t)]-4\nu\frac{\dot{R}}{R}-\frac{2\sigma}{\rho R}, \tag{1}$$

where P_g is the uniform gas pressure inside the bubble, $P_f=-P_a\sin(\omega t)$ is the forcing pressure with angular frequency ω, P_0 is the ambient pressure valid during the measurements, and the remaining parameters are material constants of the host liquid, e.g., c is the speed of sound, ρ its density, and ν is the kinematic viscosity. The gas pressure P_g can be related to $R(t)$ through an equation of state. We use a polytropic van der Waals equation of state, modified to include the effects of surface tension σ and vapor pressure P_v,

$$P_g(R(t))=\left(P_0+\frac{2\sigma}{R_0}-P_v\right)\frac{(R_0^3-a^3)^\gamma}{[R(t)^3-a^3]^\gamma}. \tag{2}$$

Here a is the hard core van der Waals radius of the gas (for argon $a=R_0/8.86$) and γ is the ratio of specific heats. In most of the acoustic period except the final stages of the collapse and after bounces, the gas can be considered isothermic [3], thus we use $\gamma=1$.

(2) Bubbles emitting light in a stable fashion contain only inert gases, and are in stable diffusive equilibrium with the surrounding liquid [18]. The points of diffusive equilibrium in the (P_a,R_0) space can be calculated from

$$C_i/C_0=\frac{\langle P_g\rangle_4}{P_0^*},\quad \langle X\rangle_i=\frac{\int_0^{T_a}R(t)^iX dt}{\int_0^{T_a}R(t)^i dt},\tag{3}$$

where $P_0^*=1$ atm is the standard atmospheric pressure and T_a is the acoustic period. For air in water, C_i is the concentration of argon set during the liquid preparation, C_0 is the tabulated dissolved air concentration of water under normal conditions. If the liquid preparation is done by degassing, then C_i can be calculated from Henry's law $C_i=0.0093C_0P_i/P_0^*$, where P_i is the partial pressure of air set during the preparation (air contains 0.93% of argon). The diffusive equilibrium is stable where the curve in the (P_a,R_0) space set by Eq. (3) is characterized by a positive slope.

(3) The acoustic pressure amplitude P_a at the bubble's position is directly proportional to the excitation voltage on the piezoelectric transmitters U_{PZT},

$$P_a=AU_{PZT}.\tag{4}$$

This assumption is reasonable when the amplitude of displacement of the resonator walls can be considered small. For values typical in SBSL experiments, $P_a<2$ bars this displacement is on the order of micrometers, thus Eq. (4) can be used safely. We define the dimensionless phase of a flash $\xi=t_{min}/T_a$ as the time elapsed from the beginning of the acoustic period until the bubble reaches its minimum radius t_{min} normalized by the acoustic period. The phase ξ that can be calculated numerically is the sum of the measured phase ξ_m and a constant parameter B, which accounts for the possible phase shift due to electronics,

$$\xi=\xi_m+B.\tag{5}$$

The phase can be measured, for instance, by displaying the photomultiplier tube (PMT) signal of the flashes and the sinusoidal excitation voltage U_{PZT} on an oscilloscope.

The detailed procedure is the following. At an experimentally known dissolved gas concentration, liquid temperature T, ambient pressure, and driving frequency, one measures $\xi_m(U_{PZT})$ at several excitation levels from the smallest possible light emission to the upper limit of SL [19]. After this, Eqs. (1)–(3) are solved systematically in a wide range of the parameters P_a and R_0, and the quantities ξ, $\langle P_g\rangle_4/P_0^*$ are extracted from the numeric $R(t)$ data. From the resulting $\xi(P_a,R_0,\langle P_g\rangle_4/P_0^*)$ data, one selects by interpolation a subset for which $\langle P_g\rangle_4/P_0^*$ equals the experimentally known value of C_i/C_0. This subset is the curve of diffusive equilibrium in the (P_a,R_0,ξ) space (see Fig. 1). The equilibrium is stable where $dR_0/dP_a>0$ or equivalently $d\xi/dP_a>0$. The final step is to fit the measured $\xi_m(U_{PZT})$ data to the stable part of the diffusive equilibrium curve in the (P_a,ξ) plane by adjusting the parameters A and B. This fit is highly constrained by the experimental fact that for a given dissolved gas concentration, the lower limit of SL is linked to the smallest P_a on the stable diffusive equilibrium curve

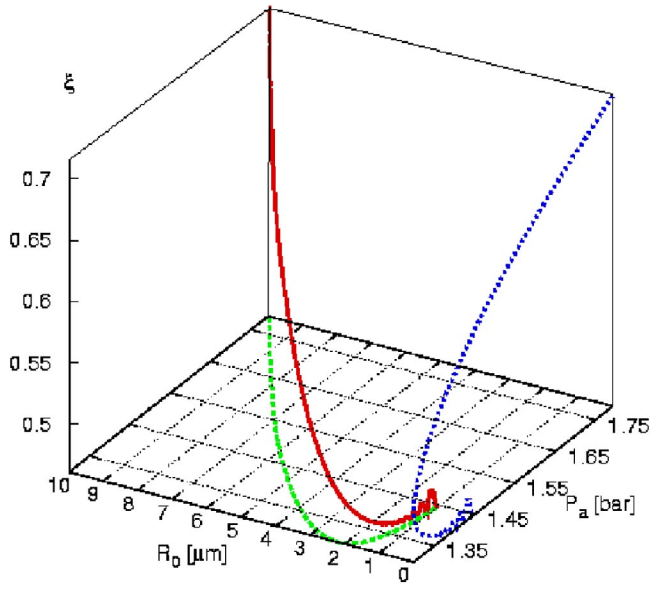

FIG. 1. The curve of diffusive equilibrium in the (P_a,R_0,ξ) space, and its projections on the (P_a,R_0) and (P_a,ξ) planes for $C_i/C_0=0.001\,35$. Stable sonoluminescing bubbles follow the stable part of this curve (where $dR_0/dP_a>0$ or $d\xi/dP_a>0$). The advantage of using the quantity ξ is that, contrary to R_0, it can be easily measured with high precision.

(see, for instance, Refs. [16,14,15]). After A and B are found, the experimental data points can also be plotted in the (P_a,R_0) plane and, in principle, $R(t)$ curves and other dynamical parameters such as the expansion ratio R_{max}/R_0 are also determined. We stress here that only those parts of the numeric $R(t)$ curves contain useful information about the size of the bubble where the assumption of isothermicity $\gamma=1$ holds. These include the expansion phase, the maximum radius, and the initial stages of the collapse, but exclude the region near the minimum radius and after bounces.

III. EXPERIMENTAL APPARATUS AND THE DETAILS OF THE MEASUREMENT

To test our method and to compare it with Mie scattering, we performed the following experiment. In a degassing equipment [21], a distilled water sample was prepared with a dissolved air concentration $0.145C_0$ at a temperature of $T=22\,^\circ$C. This corresponds to an argon concentration of $C_i=0.001\,35C_0$. The water was transferred to the resonator [21] using gravity flow. During the filling, the gas pressure in the resonator was kept at the same level as in the degassing equipment, thus no air could diffuse in or out of the water. Such care had to be taken because the precision of our method is guaranteed only if the gas concentration in the resonator is the same as set by the water preparation. After this, the resonator was placed in a setup (Fig. 2) used for recording the SL flashes and the intensities of Mie scattered laser light.

The digital oscilloscopes were triggered by the monitored driving signal U_{PZT}. For each excitation level, 54 snapshots of U_{PZT}, scattered laser intensity, and SL flashes were aver-

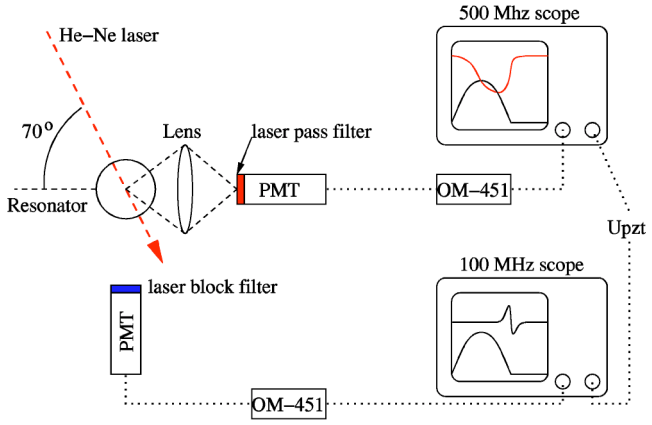

FIG. 2. The oscillating bubble was illuminated by a 30-mW He-Ne laser, and the scattered laser light was focused by a lens through an aperture into the PMT (Hamamatsu R3478). Another PMT of the same kind detected the SL flashes. The signals of the PMTs were amplified and shaped by spectroscopy amplifiers (Ortec-model 451) and visualized together with the monitored electric signal of the piezoelectric transmitters on digital oscilloscopes (HP-54616C 500 MHz, HP-54600B 100 MHz).

aged, and the resulting traces were transferred to a PC. The measurement was done at an excitation frequency of 22 700 Hz, the water temperature was $T=21.9$–$22.4\,^{\circ}\mathrm{C}$, and the external pressure $P_0=1017$ mbars. Figure 3(a) shows the fitting of the measured $\xi(U_{PZT})$ data to the calculated curve of stable diffusive equilibrium at $C_i/C_0=0.001\,35$. The error of ξ is determined by the jitter in the phase of the flashes $\approx 0.2\ \mu$s, thus $\Delta\xi\approx 0.0023$ (the time resolution was 25 ns), while the error of the pressure amplitude $\Delta P_a=0.014\,63$ bar is calculated from

$$\Delta P_a = A 2 \Delta S. \tag{6}$$

The quantity A is the proportionality constant from Eq. (4) and $\Delta S=0.001\,563V$ is the vertical resolution of the digital scope corresponding to the eight-bit digitization. Both the zero line and the maximum of the U_{PZT} signal are known with a precision of ΔS, thus there is a factor of 2 in Eq. (6). Using the calculated $\xi(P_a,R_0)$ data and the values of ξ and P_a from the fit of Fig. 3(a), one can plot the measured data points in the (P_a,R_0) plane [see the filled squares with error bars in Fig. 3(b)]. The errors of ξ and P_a determine a range of R_0 in the $\xi(P_a,R_0)$ data, which sets the error bar ΔR_0.

IV. COMPARISON WITH MIE SCATTERING

The Mie scattering method is based on the detection of laser light scattered from the bubble, whose intensity under certain conditions is proportional to the square of the radius. More precisely, the following relation holds:

$$R(t)^2=\alpha[U(t)-U_{bg}], \tag{7}$$

where $U(t)$ is the output signal of the PMT detecting the scattered intensity and U_{bg} is the background scattered intensity in the absence of the bubble. The square root of the recorded intensity is then fitted to a solution of the RP equation, and the desired parameters P_a, R_0, R_{max}, etc., are determined from the best fit. There are several difficulties of the technique that one must overcome.

(1) The scattered intensity has a very strong angle dependence. This is reduced by choosing an appropriate angle and by use of a lens that averages out the light from different angles. In our measurement we used a setup similar to that of Barber and Putterman (1992) in Ref. [10].

(2) The background scattered intensity is changing on a time scale of seconds because of small dust particles passing by near the position of the bubble due to a slow convection

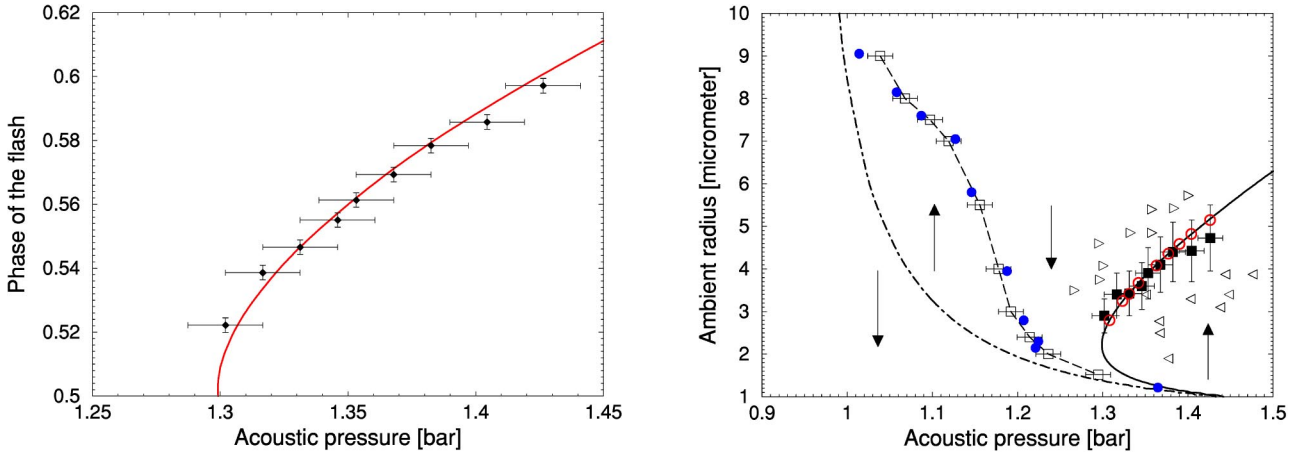

FIG. 3. The fitting of the measured phases of the flashes to the numerically calculated curve (a), and the same data (filled squares with error bars) in the (Pa,R_0) plane (b). Also in (b) the left and right triangles correspond to best fits using Mie scattering and the bounding values for the background signal. The open circles stand for the best Mie fits assuming that Eq. (3) holds precisely, while the background was allowed to vary between the bounding values. The open squares indicate best Mie fits of non-light-emitting bubbles at P_a values found from the present technique, and finally the filled circles are best Mie fits, where both P_a and R_0 were fitted. The arrows indicate regions of shrinking and growing bubbles.

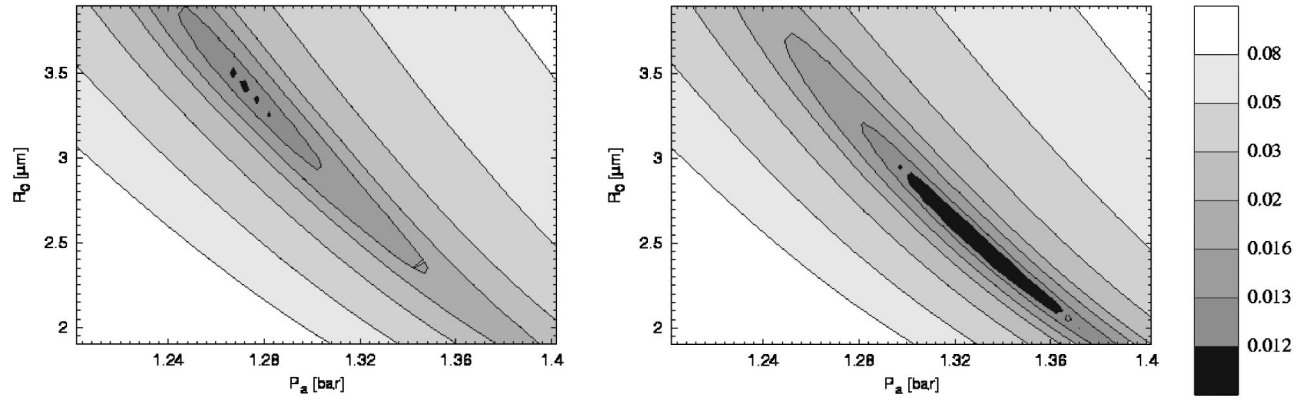

FIG. 4. The contour plots of the error of the fit Δ for the light-emitting bubble at the smallest excitation. The background level used in the fitting was $U_{bg}=-0.00\,11$ V in (a) and $U_{bg}=-0.001\,75$ V in (b). The average noise level on the intensity signal $U(t)$ corresponds to an error value $\Delta=0.013$. Fits with $\Delta\leqslant 0.013$ look good to the eye.

in the resonator. This can be handled partly by using an aperture and a laser beam as narrow as possible, but cannot be eliminated completely.

(3) Modification of the excitation level makes the bubble change its equilibrium position above the pressure antinode as the averaged Bjerkness and buoyancy forces change [22]. The intensity of the laser light in the cross section of the beam is a Gaussian, thus one always has to adjust the direction of the laser, in order to keep the bubble in the center of the beam. For this reason, the proportionality constant α in Eq. (7) may be different for each excitation level, depending on how precisely one can follow the bubble. Because of this difficulty we fitted the shape of the measured intensity signals for each excitation level, rather than using a proportionality constant found from a single fit.

We used a numeric code that accomplished the fitting automatically in a user defined range of P_a and R_0. The measured $U(t)$ curve was transformed into a normalized positive signal $u(t)=[U(t)-U_{bg}]/(U^*-U_{bg})$, where U^* is the minimum of the negative $U(t)$, which corresponds to the maximum radius of the bubble. Then a solution of the RP equation is generated at a given P_a and R_0, and the values of R_{max} and t_{min} are extracted from the numeric radius-time curve. After this, $R(t)$ was transformed into $r(t)=R(t-t_{min}+t^u_{min})/R_{max}$, where t^u_{min} is the time value of the end of the collapse in the measured $U(t)$ data. This way we got two normalized time series for which the phases corresponding to the minimum radius were identical. To be able to compare $u(t)$ and $r(t)$, these time series had to have the same number of elements, thus we interpolated $r(t)$ at time values taken from $u(t)$. Finally the difference of the signals could be characterized by a single error parameter

$$\Delta=\frac{1}{N_{min}}\sum_{i=1}^{N_{min}}|r_i^2-u_i|, \tag{8}$$

where N_{min} is the index of the minimum radius. The reason for calculating the error only until the end of the collapse is that in the after-bounce region, the assumption of $\gamma=1$ used in Eq. (2) is not valid anymore. By using this strategy for every measured $U(t)$ curve, we obtained the values of $\Delta(P_a,R_0)$ in a wide range of P_a and R_0 and thus the dynamical parameters appropriate for the smallest error could be identified. Figure 4 shows the contour plots of Δ for a particular case at two levels of the background. As can be seen, the fits are best along a line in the (P_a,R_0) space, and the fitting is very sensitive to the value of U_{bg}.

In our measurements, the precision of U_{bg} was constrained by the vertical resolution of the digital scope and the previously mentioned slow variance due to moving dust particles to $-0.0011\geqslant U_{bg}\geqslant -0.002\,25$ V. For comparison the values of U^* corresponding to the maximum radii were -0.05317 to -0.07742 V. In Fig. 4 the points within the contour $\Delta=0.013$ (which equals the noise level on the scattered intensity) determine the errors of $\Delta P_a\sim 0.04$ bar and $\Delta R_0\sim 0.7$ μm. If we also include the uncertainty of U_{bg}, then the final estimates are $\Delta P_a\sim 0.08$ bar and $\Delta R_0\sim 1$ μm. These values are consistent with the errors given by others [16,15]. The best fits with the bounding values of the background are shown in Fig. 3(b), where in the case of left and right triangles, the background was $U_{bg}=-0.0011$, and $U_{bg}=-0.002\,25$ accordingly. The filled squares found from the fitting technique of Sec. II in each case lie between the best Mie fits, confirming that these two methods provide identical results within the experimental uncertainties.

For further confirmation of the assumptions in Sec. II, we also fitted the Mie scattered data by a different strategy, where the background was allowed to vary between -0.0011 and $-0.002\,25$, and the $R(t)$ data of the fits had to satisfy Eq. (3) exactly. The best fits of this strategy are shown as open circles in Fig. 3. As can be seen, all the circles are within the error bars found from our technique. The quality of these Mie fits are also shown individually in Fig. 5.

For another independent test to confirm the assumptions of our technique, we also analyzed the measurements of U_{PZT} and Mie scattered data of non-light-emitting ''bouncing'' bubbles. The open squares with error bars in Fig. 3(b) show the case where the pressure amplitudes were calculated from Eq. (4) using the value of A found from the fitting of

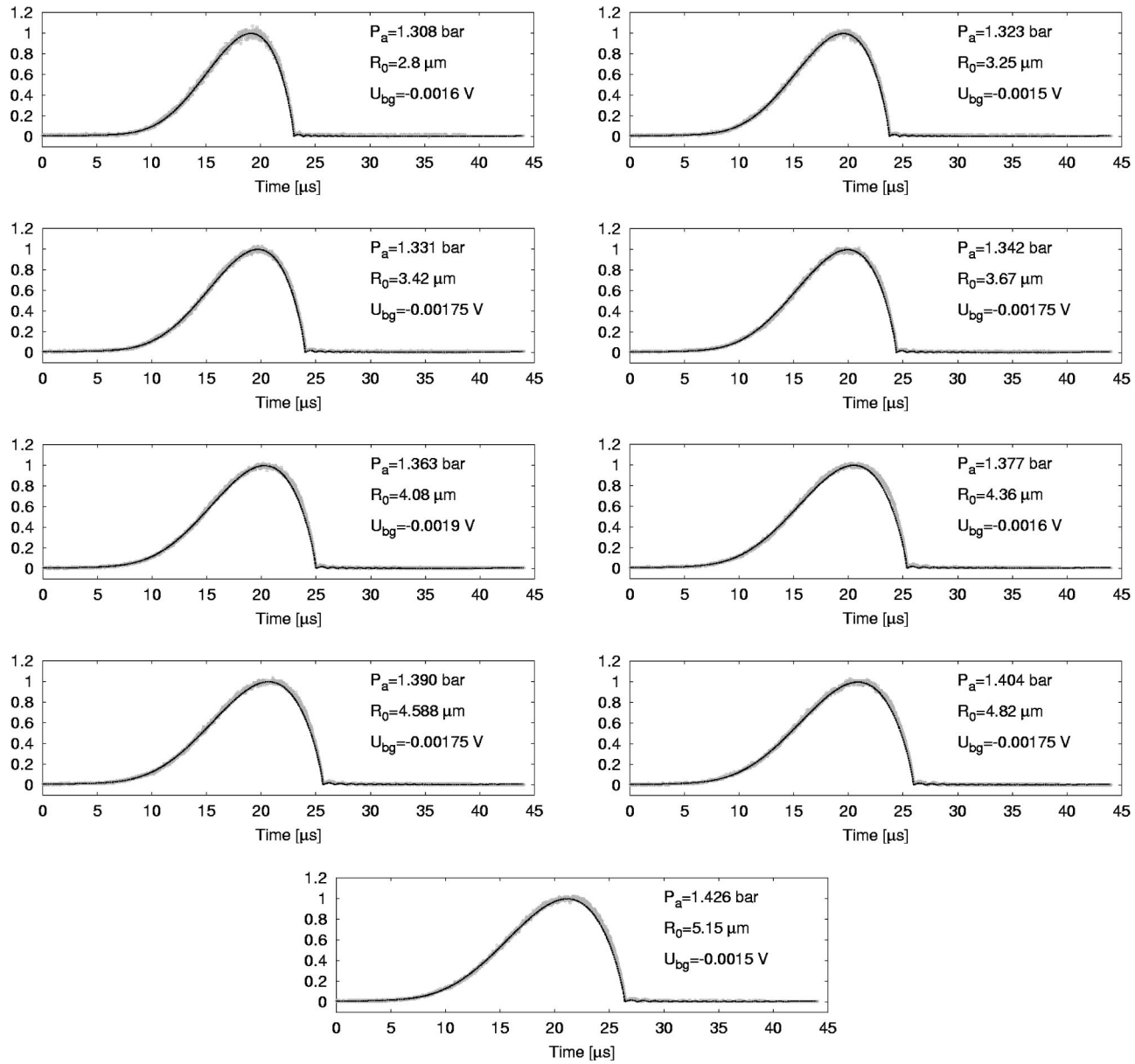

FIG. 5. The best fits of the normalized $u(t)$ and $r(t)^2$ time series corresponding to the open circles in Fig. 3(b). The parameters of the fit are indicated in the corner of the figures.

the light-emitting bubbles. The ambient radii were determined afterwards by best Mie fits at the prescribed P_a and by using the average U_{bg}. Then the fitting of the Mie scattered data is also accomplished by using the same U_{bg}, but both the P_a and R_0 parameters are allowed to vary, and the information of the U_{PZT} data is not used. The best fits using this strategy are [shown as filled circles in Fig. 3(b)] in excellent agreement with the best fits of the previous case. The phase diagram of Fig. 3(b) can also be compared to a measurement of Ref. [15], where the experimental conditions were quite close to ours (water was prepared with a dissolved air concentration of $0.14C_0$, and the excitation frequency was 20.6 KHz). The comparison with Fig. 4 of Ref. [15] shows a good quantitative agreement, further justifying our method.

V. VARIATIONS OF THE METHOD

The method described in Sec. II can also be used in slightly different forms, where only a single-fit parameter A is used, or without any unknown fit parameter, if the phase measurement is done with a hydrophone. We will briefly discuss these variations.

(1) If the experimental conditions such as the dissolved gas concentrations, liquid temperature, ambient pressure, and the material properties of the liquid are known, then the diffusive stability curve for the inert gas content in the (P_a, R_0) plane can be calculated. The point on this curve with the smallest P_a corresponds to the onset of stable SL (see Sec. IV of Ref. [17]). By measuring accurately the value of U_{PZT} at the lower threshold of SL, the unknown parameter A can

be obtained, after which the pressure amplitudes can be calculated from Eq. (4). After the pressure amplitudes of the data points are given, the corresponding R_0 values are determined by the calculated stability curve. Although, in principle, this method should work too, it is still desirable to measure the phase ξ_m together with U_{PZT}, because it provides the means of testing the self-consistency of the method and its assumptions. For instance, if the dissolved gas concentration changes considerably compared to the preset level, then the measured data (if precise enough) cannot be fitted to a simulated curve corresponding to the original gas concentration.

(2) With access to a hydrophone, one can measure the phase of the flash compared to the sinusoidal driving pressure near the bubble without the unknown parameter *B*. For this, one needs to have the aperture of the hydrophone as close to the bubble as possible and detect the pressure variations during an acoustic cycle together with the spike reminiscent of the shock wave launched by the bubble at its minimum radius. Although the finite propagation time of the shock wave will introduce a small phase shift, it should be possible to account for this effect by using a model for shock propagation [as in Ref. [8] (1998)] and measuring the distance to the bubble either by the pulse-echo method of Ref. [20] or by a microscope as in Ref. [8] (1997). From the measured phase and the calculated diffusive stability curve, one can then work backwards and find the corresponding P_a and R_0 values. If the hydrophone is pressure calibrated, then the deduced P_a values can also be compared to the measured P_a, providing a test of self-consistency. This method, although highly intrusive and more difficult to carry out than that described in Sec. II has the advantage that it does not involve the fitting of unknown parameters and thus could serve as a good additional test experiment to the original method.

VI. CONCLUSION

In this paper we presented an alternative method for the deduction of important dynamical parameters of SBSL, namely, the pressure amplitude P_a, the ambient radius R_0, and the expansion ratio R_{max}/R_0. The method is based on previously confirmed theoretical assumptions and the measurement of the phase of the flashes in the acoustic period together with the driving signal on the piezoelectric transmitters and the precise knowledge of the experimental conditions, especially the dissolved gas concentration in the liquid. We demonstrated the method by measuring the P_a and R_0 parameters of light-emitting bubbles for a given argon concentration. At the same time, measurements of these parameters were also done by the conventional Mie scattering method, revealing that within experimental uncertainties, these two approaches produced identical results. The phase diagram obtained is in good quantitative agreement with that of Ref. [15]. The limitation of the method is that, unlike Mie scattering, it cannot be used to measure non-light-emitting bubbles, and is also unable to measure unstable SL. However the important advantage of the method is its *noninvasive* chararcter, and thus its applicability to situations where the other methods are either impractical or even potentially destructive to use as, e.g., in single-photon correlation measurements or in measuring the parametric dependence of SBSL spectra. Moreover, the technique does not require expensive apparatus other than a digital oscilloscope and a PMT, and the data analysis is easily automatized.

ACKNOWLEDGMENTS

The authors acknowledge financial support by the Danish Nonlinear School and the Danish National Science Foundation. G.S. also thanks ERASMUS for financial support.

[1] B.P. Barber *et al.*, Phys. Rep. **281**, 65 (1997); M.P. Brenner, S. Hilgenfeldt, and D. Lohse, Rev. Mod. Phys. **74**, 425 (2002).

[2] D. F. Gaitan, Ph.D. thesis, University of Mississippi, 1990 (unpublished); S.J. Putterman, Sci. Am. **272**(2), 32 (1995).

[3] A. Prosperetti, J. Acoust. Soc. Am. **61**, 17 (1977); A. Prosperetti, J. Fluid Mech. **222**, 587 (1991); K. Yasui, J. Acoust. Soc. Am. **98**, 2772 (1995); M.-C. Chu and D. Leung, J. Phys.: Condens. Matter **9**, 3387 (1997).

[4] A. Eller and H.G. Flynn, J. Acoust. Soc. Am. **37**, 493 (1965); M.M. Fyrillas and A.J. Szeri, J. Fluid Mech. **277**, 381 (1994); R. Löfstedt, K. Weninger, S. Putterman, and B.P. Barber, Phys. Rev. E **51**, 4400 (1995); M.P. Brenner, D. Lohse, D. Oxtoby, and T.F. Dupont, Phys. Rev. Lett. **76**, 1158 (1996); P.H. Roberts and C.C. Wu, J. Theoret. Comput. Fluid Dynamics **10**, 357 (1998).

[5] D. Lohse, M.P. Brenner, T.F. Dupont, S. Hilgenfeldt, and B. Johnston, Phys. Rev. Lett. **78**, 1359 (1997); D. Lohse and S. Hilgenfeldt, J. Chem. Phys. **107**, 6986 (1997); K. Yasui, J. Phys. Soc. Jpn. **66**, 2911 (1997).

[6] A. Prosperetti, Q. Appl. Math. **34**, 339 (1977); M.P. Brenner, D. Lohse, and T.F. Dupont, Phys. Rev. Lett. **75**, 954 (1995); S. Hilgenfeldt, D. Lohse, and M.P. Brenner, Phys. Fluids **8**, 2808 (1996); C.C. Wu and P.H. Roberts, Phys. Lett. A **250**, 131 (1998); A. Prosperetti and Y. Hao, Philos. Trans. R. Soc. London, Ser. A **357**, 203 (1999); U.H. Augsdörfer, A.K. Evans, and D.P. Oxley, Phys. Rev. E **61**, 5278 (2000); B.D. Storey, *ibid.* **64**, 017301 (2001).

[7] W. Lauterborn and E. Suchla, Phys. Rev. Lett. **53**, 2304 (1984); W. Lauterborn and A. Koch, Phys. Rev. A **35**, 1974 (1987); P. Smereka, B. Birnir, and S. Banerjee, Phys. Fluids **30**, 3342 (1987); U. Parlitz, V. Englisch, C. Scheffczyk, and W. Lauterborn, J. Acoust. Soc. Am. **88**, 1061 (1990); R.G. Holt, D.F. Gaitan, A.A. Atchley, and J. Holzfuss, Phys. Rev. Lett. **72**, 1376 (1994); G. Simon *et al.*, Nonlinearity **15**, 25 (2002).

[8] T.J. Matula, I.M. Hallaj, R.O. Cleveland, and L.A. Crum, J. Acoust. Soc. Am. **103**, 1377 (1997); J. Holzfuss, M. Rüggeberg, and A. Billo, Phys. Rev. Lett. **81**, 5434 (1998); R. Pecha and B. Gompf, *ibid.* **84**, 1328 (2000).

[9] B.P. Barber and S.J. Putterman, Nature (London) **352**, 318 (1991); R. Pecha, B. Gompf, G. Nick, Z.Q. Wang, and W.

Eisenmenger, Phys. Rev. Lett. **81**, 717 (1998); B.P. Barber, C.C. Wu, R. Löfstedt, P.H. Roberts, and S.J. Putterman, *ibid.* **72**, 1380 (1994); R. Hiller, S.J. Putterman, and B.P. Barber, *ibid.* **69**, 1182 (1992); W.C. Moss *et al.*, Phys. Rev. E **59**, 2986 (1999); S. Hilgenfeldt, S. Grossmann, and D. Lohse, Phys. Fluids **11**, 1318 (1999).

[10] B.P. Barber and S.J. Putterman, Phys. Rev. Lett. **69**, 3839 (1992); W.J. Lentz, A.A. Atchley, and D.F. Gaitan, Appl. Opt. **34**, 2648 (1995); K.R. Weninger, B.P. Barber, and S.J. Putterman, Phys. Rev. Lett. **78**, 1799 (1997); K.R. Weninger, P.G. Evans, and S.J. Putterman, Phys. Rev. E **61**, 1020 (2000); B. Gompf, and R. Pecha, *ibid.* **61**, 5253 (2000).

[11] Y.J. Tian, J.A. Ketterling, and R.E. Apfel, J. Acoust. Soc. Am. **100**, 3976 (1996).

[12] G. Vacca, R.D. Morgan, and R.B. Laughlin, Phys. Rev. E **60**, 6303 (1999).

[13] G.A. Delgadino and F.J. Bonetto, Phys. Rev. E **56**, R6248 (1997).

[14] R.G. Holt and D.F. Gaitan, Phys. Rev. Lett. **77**, 3791 (1996).

[15] D.F. Gaitan and R.G. Holt, Phys. Rev. E **59**, 5495 (1999).

[16] J.A. Ketterling and R.E. Apfel, Phys. Rev. Lett. **81**, 4991 (1998); J.A. Ketterling and R.E. Apfel, J. Acoust. Soc. Am. **107**, L13 (2000); J.A. Ketterling and R.E. Apfel, Phys. Rev. E **61**, 3832 (2000).

[17] G. Simon, I. Csabai, Á. Horváth, and F. Szalai, Phys. Rev. E **63**, 026301 (2001).

[18] This assumption is the direct consequence of chemical reactions [5] and diffusion, and it was confirmed experimentally in Refs. [20,16,14,15].

[19] At high degassing, a hysteresis in the lower SL threshold can be observed (see the work of Lohse and Hilgenfeldt in Ref. [5]). In these cases the state with the smallest light emission should be approached from above to obtain the true values of the lower SL threshold.

[20] T.J. Matula and L.A. Crum, Phys. Rev. Lett. **80**, 865 (1998).

[21] The detailed description of the experimental apparatus and procedures will be available in G. Simon, Ph.D. thesis, Eötvös University, 2003 (unpublished).

[22] T.J. Matula, S.M. Cordry, R.A. Roy, and L.A. Crum, J. Acoust. Soc. Am. **102**, 1522 (1997).